Preferential fluid flow and chemical transport in saturated fractured porous media and in heterogeneous vadose zones: Two sides of the same coin

Brian Berkowitz
Department of Earth and Planetary Sciences, Weizmann Institute of Science, Rehovot 7610001, Israel

Notes for discussion:

- Preferential fluid flow and chemical transport occur on scales ranging from pores to entire aquifers, in both fully and partially water-saturated geological formations.
- Preferential flows can be considered, in a general sense, manifestations of self-organization that hinders perfect mixing within a system, and leads to faster throughput of water and chemicals.
- At least some conceptualizations and quantitative characterizations of preferential fluid flow and chemical transport in porous and fractured systems – both saturated and partially saturated – can be unified in terms of tools that connect them in a dynamic framework.

Some illustrations below.

➔ Even well-connected fracture networks can display highly non-uniform preferential paths for fluid and chemicals (Margolin et al., 1998; Copyright American Geophysical Union 1998, All Rights Reserved). Highly connected networks with large variances in apertures of pores/fractures can exhibit flow dominated by a few preferential pathways.

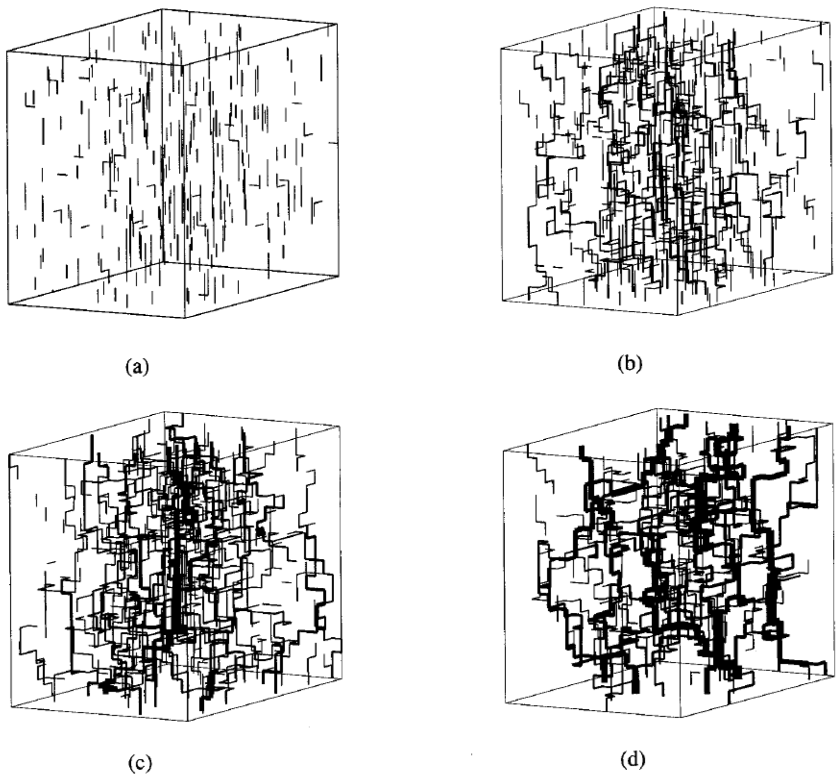

Figure 3. Typical spatial distributions of normalized bond discharges in three dimensions for different values of b (isotropic network, $p = 0.5$, and $L = 20$): (a) $b = 0.0$; 400 bonds are shown, with discharges of 1.0%–2.2% of Q_{tot}; (b) $b = 0.5$; 1242 bonds are shown, with discharges of 1.0%–4.9% of Q_{tot}; (c) $b = 1.0$; 1507 bonds are shown, with discharges of 1.0%–15.9% of Q_{tot}; and (d) $b = 2.0$; 1329 bonds are shown, with discharges of 1.0%–20.4% of Q_{tot}. The thicknesses of the bonds are proportional to the relative discharges they carry.

➔ This behavior is similar to that of (rapid) infiltration in soils and the vadose zone, which exhibits strongly localized preferential pathways in root channels, cracks, worm burrows or connected inter-aggregate pore networks (Gouet-Kaplan and Berkowitz, 2011; Copyright Soil Science Society of America 2011, All Rights Reserved).

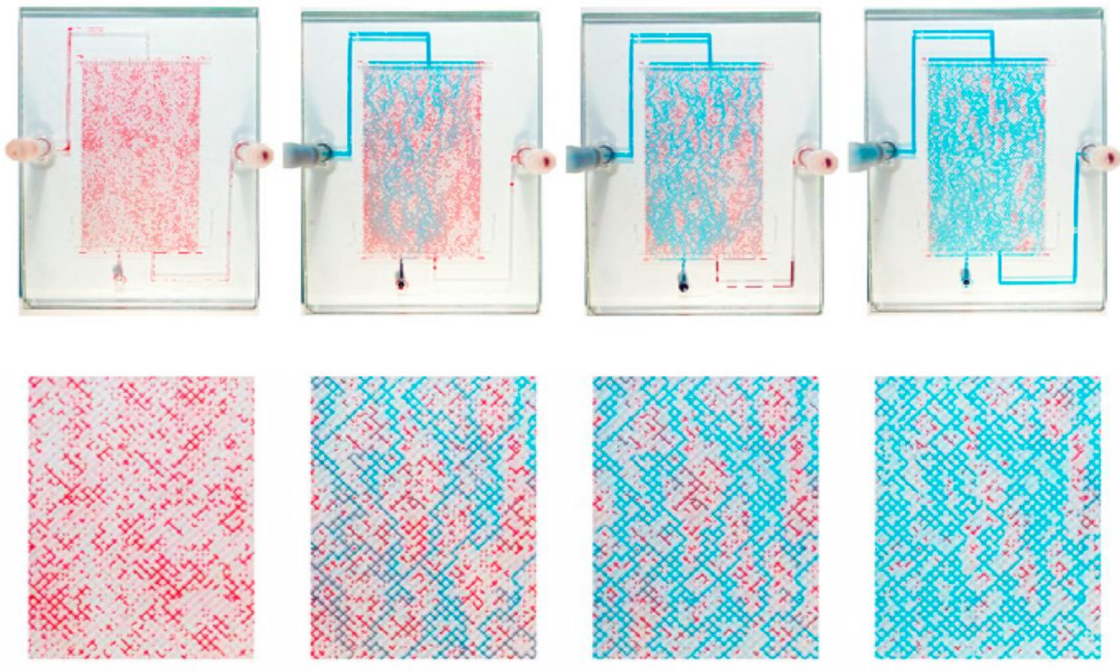

Fig. 2. Typical processing result for new water infiltration (blue) in the lattice micromodel partially saturated by old water (red). Infiltrating flow is from top to bottom; from left to right, the partial displacement of the red dye can be followed in time. Purple regions indicate mixing of the old and new water. Note that some clusters of red dye remain uncontaminated by blue dye while others are mixed, i.e., the preferential flow of new water leaves some pockets of old water intact even after flow of blue dye reaches steady state at the outlet. Top pictures show entire micromodel with inlet and outlet; bottom pictures show a detailed area. These specific pictures are from a preliminary run, and the order of the dyes differs from the results discussed.

➔ Vadose domain (and fracture networks) can display "memory effects", in terms of the location and functioning of preferential paths even during perturbations in the velocity gradient and/or rates of infiltration (Kapetas et al., 2014).

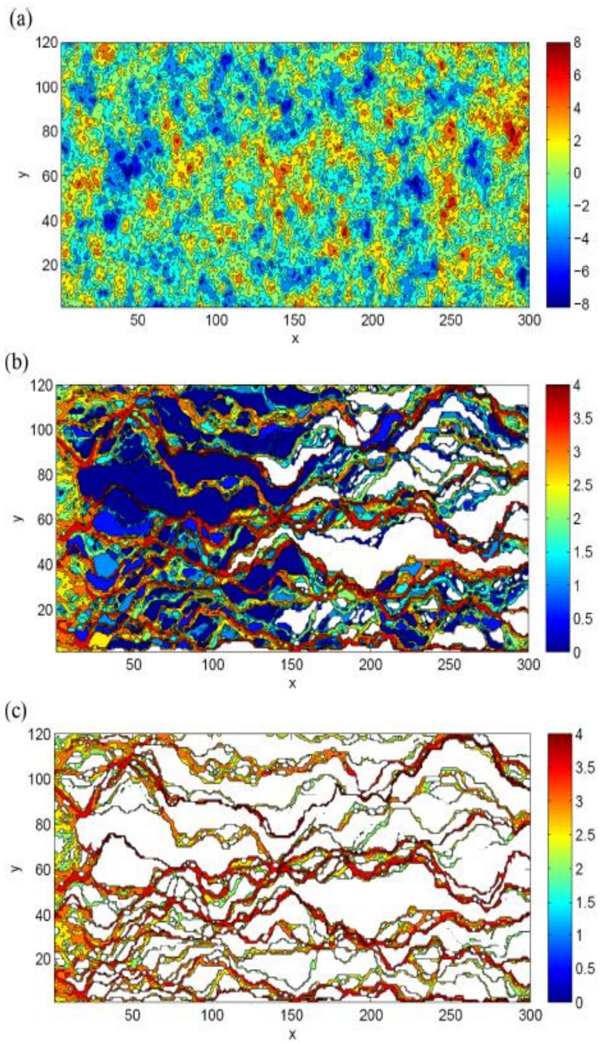

Figure 4. **(a)** Spatial map showing a sample hydraulic conductivity (K) field generated statistically (right side bar shows scale of $\ln(K)$). **(b)** Spatial map showing particle paths through the domain, for overall hydraulic gradient (water flow) from left to right. "Particles" representing dissolving chemical species are injected along the left vertical boundary and followed through the domain. White regions indicate where *no* particles "visit" (interrogate) the domain. Blue regions have only a small number of particle visitations. Red regions have significant particle visitations. Note that the colour bar is in log10 number of particles. **(c)** Spatial map showing *preferential* particle paths, defined as paths through cells (underlying subdivisions in the domain, each with a different K value as shown in panel **a** above) that each contain a "visitation" of a minimum of 0.1 % of the total number of particles in the domain. Note that the colour bar is in log10 number of particles (after Edery et al., 2014; © with permission from the American Geophysical Union 2014).

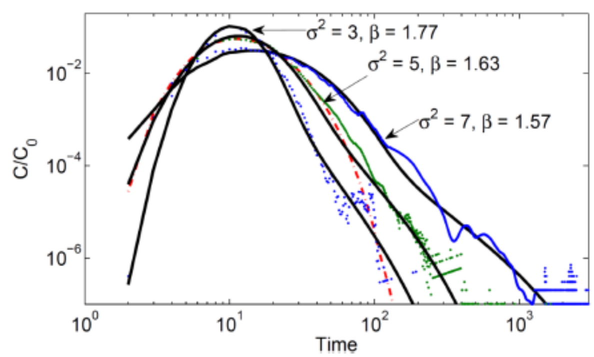

Figure 5. Breakthrough curves (points) for three $\ln(K)$ variances ($\sigma^2 = 3, 5, 7$; 100 realizations each), at the domain outlet ($x = 300$ length units), and corresponding CTRW fits (curves). Also shown is a fit of the advection–dispersion equation (dashed–dotted curve), for $\sigma^2 = 5$. See Sect. 3.3 for further discussion and explanation of β. All values are in consistent, arbitrary length and time units (after Edery et al., 2014; © with permission from the American Geophysical Union 2014).

➔ The ubiquity of unresolved (or uncharacterized) heterogeneity at all spatial and temporal scales necessitates the use of effective medium models that enable an accounting of a wide range of flow and transport behaviors. For chemical transport, we use the Continuous Time Random Walk (CTRW) framework (Berkowitz et al., 2006, 2016) focus on a probabilistic modelling framework that can capture the dynamics in heterogeneous vadose zones and fractured (or otherwise heterogeneous) geological formations (Edery et al., 2014; Copyright American Geophysical Union 2014, All Rights Reserved).

➔ Application of this model interprets field-scale tracer breakthrough curves (concentration vs. time) in a highly fractured karst formation over length scales of up to more than 7 km (Goeppert et al., 2020; Copyright Elsevier 2020).

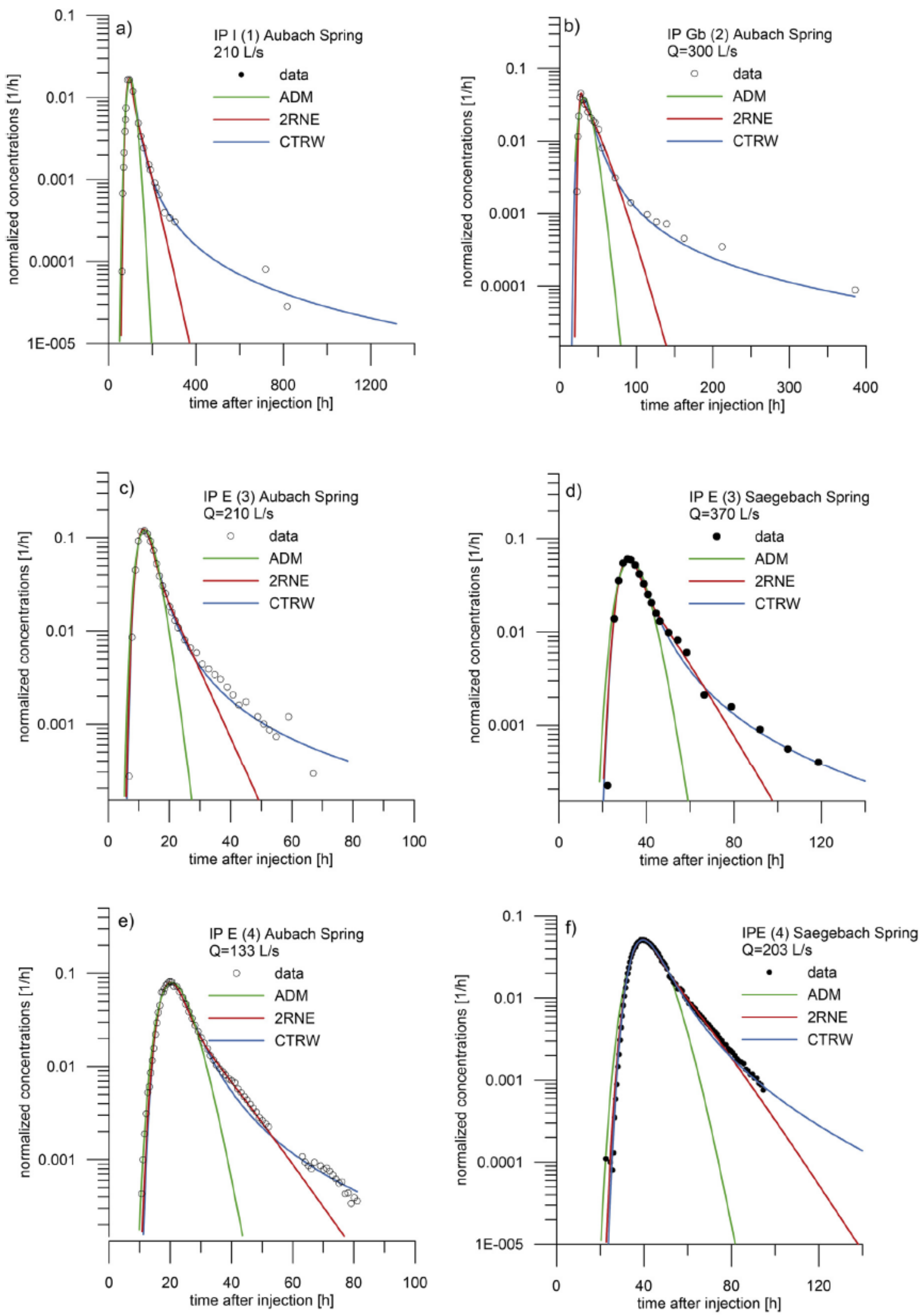

Fig. 2. Observed and modeled BTCs with individual peak fits of CTRW, ADE and 2RNE. Selected BTCs for the injection and outlet locations at (a) Iferflucht (IP I – 1) and A
Spring, (b) Geissbuehl (IP Gb – 2) and Aubach Spring, (c) the estavelle (IP E – 3) and Aubach Spring and (d) Saegebach Spring and under different flow conditions for IP E –
Aubach Spring and (f) Saegebach Spring. Normalized concentrations are obtained by dividing the concentrations C by the recovered tracer mass and multiplying by the me
discharge.

Specific literature:

Margolin, G., B. Berkowitz and H. Scher (1998). Structure, flow, and generalized conductivity scaling in fracture networks, *Water Resources Research*, 34(9), 2103-2121, doi:10.1029/98WR01648

Gouet-Kaplan, M. and B. Berkowitz (2011). Measurements of interactions between resident and infiltrating water in a lattice micromodel, *Vadose Zone Journal*, 10, 624-633, doi:10.2136/vzj2010.0103.

Kapetas, L., I. Dror and B. Berkowitz (2014). Evidence of preferential path formation and path memory effect during successive infiltration and drainage cycles in uniform sand columns, *Journal of Contaminant Hydrology*, 165, 1-10, doi:10.1016/j.jconhyd.2014.06.016.

Berkowitz, B., A. Cortis, M. Dentz and H. Scher (2006). Modeling non-Fickian transport in geological formations as a continuous time random walk, *Reviews of Geophysics*, 44, RG2003, doi:10.1029/2005RG000178.

Berkowitz, B., I. Dror, S.K. Hansen and H. Scher (2016). Measurements and models of reactive transport in geological media, *Reviews of Geophysics*, 54, 930-986, doi:10.1002/2016RG000524.

Edery, Y., A. Guadagnini, H. Scher and B. Berkowitz (2014). Origins of anomalous transport in disordered media: Structural and dynamic controls, *Water Resources Research*, 50, 1490-1505, doi:10.1002/2013WR015111.

Goeppert, N., N. Goldscheider, and B. Berkowitz (2020) Experimental and modeling evidence of kilometer-scale anomalous tracer transport in an alpine karst aquifer, *Water Research*, 178, 115755, doi:10.1016/j.watres.2020.115755.